

# Effect of Interfacial Microstructure Evolution on Mechanical Properties and Fracture Behavior of Friction Stir-Welded Al-Cu Joints



P. XUE, B.L. XIAO, and Z.Y. MA

The interfacial microstructure evolution of Al-Cu joints during friction stir welding and post-welding annealing and its influence on the tensile strength and the fracture behavior were investigated in detail. An obvious interface including three sub-layers of  $\alpha$ -Al,  $\text{Al}_2\text{Cu}$ , and  $\text{Al}_4\text{Cu}_9$  intermetallic compound (IMC) layers is generated in the as-FSW joint. With the development of annealing process, the  $\alpha$ -Al layer disappeared and a new IMC layer of AlCu formed between initial two IMC layers of  $\text{Al}_2\text{Cu}$  and  $\text{Al}_4\text{Cu}_9$ . The growth rate of IMC layers was diffusion controlled before the formation of Kirkendall voids, with activation energy of 117 kJ/mol. When the total thickness of IMC layers was less than the critical value of 2.5  $\mu\text{m}$ , the FSW joints fractured at the heat-affected zone of Al side with a high ultimate tensile strength (UTS) of  $\sim 100$  MPa. When the thickness of IMC layers exceeded 2.5  $\mu\text{m}$ , the joints fractured at the interface. For relatively thin IMC layer, the joints exhibited a slightly decreased UTS of  $\sim 90$  MPa and an inter-granular fracture mode with crack propagating mainly between the  $\text{Al}_2\text{Cu}$  and AlCu IMC layers. However, when the IMC layer was very thick, crack propagated in the whole IMC layers and the fracture exhibited trans-granular mode with a greatly decreased UTS of 50-60 MPa.

DOI: 10.1007/s11661-015-2909-1

© The Minerals, Metals & Materials Society and ASM International 2015

## I. INTRODUCTION

IN recent years, dissimilar joints are increasingly being used in industrial applications due to their numerous advantages.<sup>[1-9]</sup> Copper and aluminum are two common metals that are widely used in the electrical industries. Due to the low density and the low cost, aluminum is being widely applied in place of copper except in some key devices, such as the terminal board which needs bolt fastening.<sup>[10]</sup> This inevitably involves the dissimilar joining of aluminum and copper.

Dissimilar metals are difficult to be joined with the conventional fusion welding methods due to their different chemical and physical characteristics.<sup>[9]</sup> Therefore, many solid-state joining methods, such as friction welding (FW), cold rolling welding (CRW), and explosive welding (EW), have received much attention.<sup>[3-5,11-17]</sup> These methods, however, have a few drawbacks. For example, FW and RW lack versatility, and EW involves in the safety problems.

In the past decade, much attention has been drawn to the friction stir welding (FSW) of dissimilar materials, due to its various advantages, like the low distortion, energy efficiency, versatility and so on.<sup>[18,19]</sup> Various dissimilar joints have been successfully prepared *via*

FSW, and excellent tensile and bending properties could be achieved in the Al-Cu joints at proper FSW parameters.<sup>[6,20-28]</sup>

It should be emphasized that intermetallic compounds (IMCs) were easy to form in the dissimilar joints prepared by FSW and other solid-state joining methods, forming an IMC layer at the interface.<sup>[1-17,20-28]</sup> During the service life of the Al-Cu joints, the frequent current surges on the network may generate favorable conditions for annealing effect.<sup>[4,11]</sup> This will enhance the interdiffusion between Al and Cu, resulting in the further development of IMCs at the initial interface. Therefore, it is necessary to clarify the evolution of the IMCs at the interface during the interdiffusion process, since the brittle IMC phases can be detrimental to the reliability of the dissimilar joints in practical applications.

During the past decades, the evolution of the layered IMC phases at the interface during annealing process in various Al-Cu joints and diffusion couples has been investigated by many researchers.<sup>[4,5,10-16]</sup> However, there is no general consensus on the formation of IMCs, and thus further investigation on the IMC evolution during interdiffusion are still needed due to the complex reaction process between Al and Cu.

According to the Al-Cu binary phase equilibrium diagram,<sup>[29]</sup> eight types of IMC phases may possibly develop in the Al-Cu system. However, besides the chemical potentials, the formation of IMC phases also depends on the initial nucleation conditions and the mobilities of the constituent elements during solid-state interdiffusion process, which is different from the

P. XUE, Assistant Professor, and B.L. XIAO and Z.Y. MA, Professors, are with the Shenyang National Laboratory for Materials Science, Institute of Metal Research, Chinese Academy of Sciences, 72 Wenhua Road, Shenyang 110016, P.R. China. Contact e-mail: zyma@imr.ac.cn

Manuscript submitted December 3, 2014.

Article published online April 21, 2015

equilibrium solidification process.<sup>[2,30]</sup> So, not all the IMC phases in the equilibrium phase diagram necessarily form during interdiffusion process.

The mechanical properties of the Al-Cu joints are dramatically affected by the formation and growth of the IMCs at the interface.<sup>[10,11]</sup> A thin IMC layer is an essential requirement for good metallurgical bonding of the dissimilar joints,<sup>[22–24]</sup> while excessive IMCs would increase the brittleness of the interface and seriously impair the overall mechanical integrity.<sup>[5,12,14,15]</sup> Chen *et al.*<sup>[5]</sup> suggested that the fracture morphology of the Al-Cu joints changed from ductile damage to brittle cleavage with increasing the thickness of the IMC layers. For the FSW Al-Cu joints, excessive IMCs easily form at the interface and the nugget zone (NZ), resulting in reduced mechanical properties.<sup>[22–28]</sup>

Although many studies have been performed on the interfacial IMC growth in the Al-Cu dissimilar joints, fine microstructure of the IMC layer and its effect on the mechanical behavior are still lacking, especially for the FSW Al-Cu joints. In the present study, the FSW Al-Cu joints under both as-FSW and subsequent annealing conditions were subjected to detailed microstructure examination and property test. This study aims at (a) to elucidate the microstructural evolution of the interface of Al-Cu joints during FSW and subsequent annealing; (b) to establish the growth kinetics of IMC layers during annealing treatment; and (c) to clarify the influence of the development of IMC layers on the mechanical properties and fracture behavior of the Al-Cu joints.

## II. EXPERIMENTAL PROCEDURES

1060 aluminum and commercial pure copper (99.9 pct purity) plates 5 mm in thickness, 300 mm in length, and 70 mm in width were butt-welded using a gantry FSW machine (China FSW Center, China). Unlike the conventional FSW, the tool pin should mostly offset into the softer material side in order to obtain defect-free joints when FSW of dissimilar materials.<sup>[22–28]</sup> Therefore, the pin stirred mainly in the aluminum during FSW process. The welding tool used in this study was made of heat-treated tool steel and had a shoulder 20 mm in diameter and a pin 6 mm in diameter and 4.8 mm in length. FSW was performed with a counter clock-wisely rotating pin at a tool rotation rate of 600 rpm and a traverse speed of 100 mm/min. The annealing treatments of the Al-Cu joints were carried out at 523 K and 673 K (250 °C and 400 °C) for 1-6 days and 0.5-12 hours in electrical furnace, respectively.

Microstructure of the FSW joints was observed on a Leica MEF4A optical microscopy (OM; Leica Corporation, Germany), and the detailed microstructural characterization and analyses of the interface were performed on a Shimadzu EPMA-1610 electron probe microscopic analyzer (EPMA; Shimadzu Corporation, Japan), a Zeiss Supra 35 field-emission gun scanning electron microscopy (SEM; Zeiss Corporation, Germany), and a FEI Tecnai G2 20 transmission electron microscopy (TEM; FEI Corporation, Hillsboro, OR), complemented by energy-dispersive spectroscopy

(EDS). The growth rate of the IMC phases was determined by measuring the thickness of the interdiffusion layers from their backscattered electron images (BEI) by SEM.

For the IMC layer in the Al-Cu joints annealed at 523 K (250 °C) with a relatively small thickness, the microstructure observation and phase identification were carried out on TEM. The TEM specimens were prepared from slices ~600  $\mu\text{m}$  in thickness, cut from the joint perpendicular to the welding direction with the interface approximately passing through the slice center. These slices were ground to a thickness of ~40  $\mu\text{m}$  and finally polished on a Gatan 691 type ion-milling device after pitting.

Transverse tensile specimens with a gage length of 40 mm and a width of 10 mm were machined perpendicular to the FSW direction. Tensile tests were carried out on a Zwick/Roell Z050 tensile test machine at an initial strain rate of  $1 \times 10^{-3} \text{ s}^{-1}$ , and at least two specimens were tested for each sample type. A Rigaku D/Max-2500PC X-ray diffractometer (XRD) was then used to identify the phases on the fracture surfaces of both the Cu side and Al side. The observations of the surface morphology and the path of crack propagation were carried out on SEM.

## III. RESULTS

### A. Microstructure of the Interface in as-FSW Al-Cu Joint

Figure 1 shows the OM macroscopic appearance of the as-FSW Al-Cu joint and the microstructure of the interface. As shown in Figure 1(a), the NZ exhibited a mixture of the Al matrix and Cu particles. Between the NZ and the Cu base metal (BM), a distinct border, *i.e.*, the Al-Cu interface, could be observed. As shown in the SEM microstructure of Figure 1(b), a continuous and uniform interface layer with a thickness of ~1  $\mu\text{m}$ , consisting of two sub-layers, was clearly observed between Al and Cu BM. Detailed TEM bright field image of the interface layer is shown in Figure 1(c). Different from the SEM results, three discernible sub-layers (defined as layers A, B, and C, respectively) could be observed. Among these three layers, layer A was discontinuous; layers B and C were continuous, corresponding to the two sub-layers observed in Figure 1(b).

Figure 2 shows the detailed microstructure of each sub-layer in the as-FSW Al-Cu interface. As shown in Figure 2(a), high density of dislocations existed in layer A. According to the selected area diffraction (SAD) pattern shown in the upper-right corner, layer A was identified as Al. EDS results indicated that layer A contained ~1.6 at. pct Cu, which was much higher than that in the Al matrix of the NZ with ~0.8 at. pct Cu. Therefore, the discontinuous layer A was the Al-based supersaturated solid solution. Figure 2(b) indicates that the grains in layer B exhibited columnar characteristic, and were identified as  $\text{Al}_2\text{Cu}$  according to the EDS results and the SAD patterns. The grains in layer C exhibited an irregular shape, and most grains were

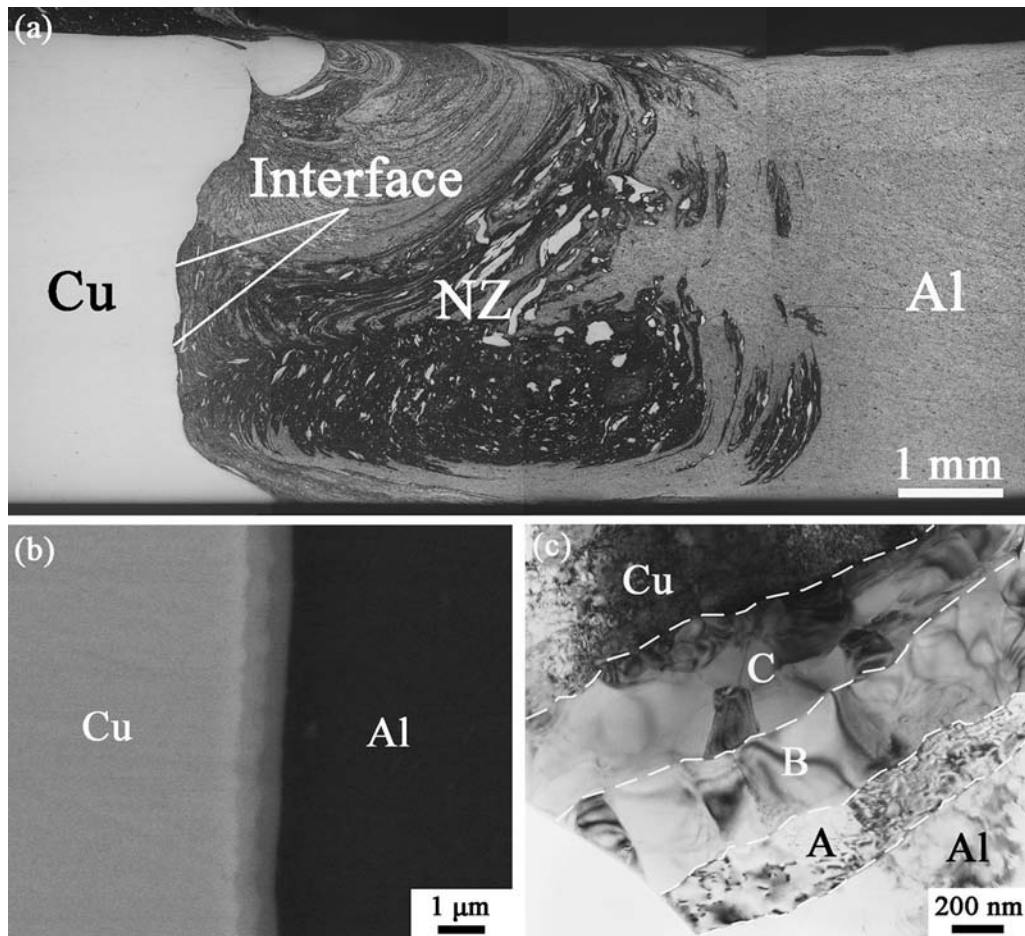


Fig. 1—(a) Optical macrostructure of as-FSW Al-Cu joint, microstructure of Al-Cu interface for (b) SEM backscattered electron image (BEI), and (c) TEM bright field image.

identified as  $\text{Al}_4\text{Cu}_9$  according to the SAD patterns (Figure 2(c)). Moreover, few fine  $\text{AlCu}$  grains were also observed in this layer, and their typical microstructure and SAD pattern were shown in Figure 2(d).

### B. Microstructure Evolution of the Interface During Annealing

Figure 3 shows the evolution of the interfacial structure for the FSW Al-Cu joints under various annealing conditions. At a relatively low annealing temperature of 523 K (250 °C) for 1 day, the Al-Cu interface exhibited almost the same microstructure as the original structure, while the thickness increased a little (Figure 3(a)). However, as the annealing time increased further to 3 and 6 days, a new IMC layer formed and grew between the initial two IMC layers (Figures 3(b) and (c)), resulting in a sandwich structure of IMC layers at the Al-Cu interface. Meanwhile, the  $\text{Al}_2\text{Cu}$  and  $\text{Al}_4\text{Cu}_9$  IMC layers also grew obviously with the increasing annealing time. It should be pointed out that many  $\text{Al}_2\text{Cu}$  particles appeared in the NZ,<sup>[22]</sup> which were bonded into the  $\text{Al}_2\text{Cu}$  IMC layer during the interface development in annealing process, as shown in Figure 3(b).

When annealed at 673 K (400 °C), the sandwich structure of IMC layers could be observed just after an hour, as shown in Figure 3(d). Then, each layer in the sandwich structure grew with the increasing annealing time. After annealed at 673 K (400 °C) for 9 hours, some Kirkendall voids could be observed between the  $\text{Al}_4\text{Cu}_9$  IMC layer and the Cu BM (Figure 3(e)). When the annealing time was increased to 11 h, more and more Kirkendall voids formed and connected with each other, forming a Kirkendall tunnel, as shown in Figure 3(f).

Figure 4 shows the detailed TEM microstructure of the Al-Cu interface after annealed at 523 K (250 °C). For the Al-Cu interface annealed at 523 K (250 °C) for 3 days (Figure 4(a)), the initial  $\alpha$ -Al supersaturated solid solution layer disappeared and the columnar grains still existed in the  $\text{Al}_2\text{Cu}$  IMC layer. However, these columnar grains were gradually replaced by the equiaxed  $\text{Al}_2\text{Cu}$  grains generated near the Al matrix. The microstructure of  $\text{Al}_4\text{Cu}_9$  IMC layer was not changed except for that more equiaxed grains were generated, resulting in the increased IMC thickness. Between the  $\text{Al}_2\text{Cu}$  and  $\text{Al}_4\text{Cu}_9$  IMC layers, a new IMC layer consisting of  $\text{AlCu}$  with a grain size of  $\sim 200$  nm began to generate from the  $\text{Al}_4\text{Cu}_9$  IMC layer, while the



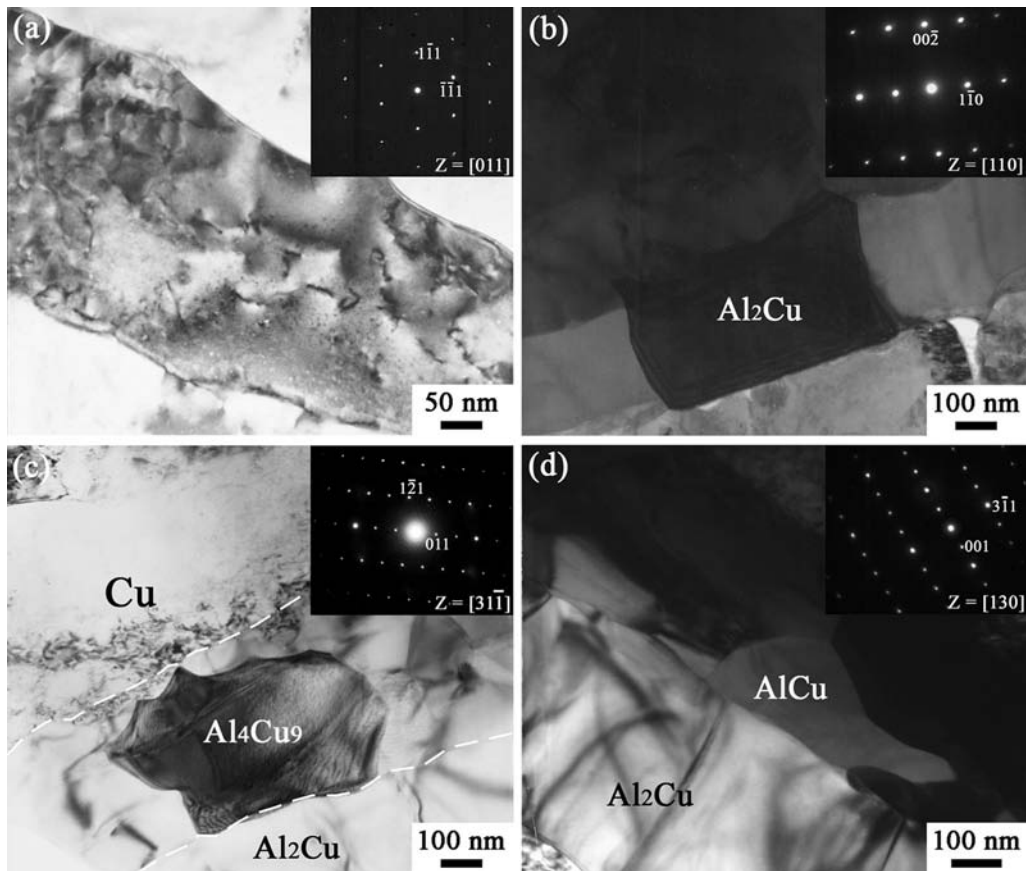


Fig. 2—TEM images showing microstructures of (a) layer A, (b) layer B, (c), and (d) layer C in Fig. 1(c).

boundary was not clear; however, obvious border existed between the  $\text{Al}_2\text{Cu}$  and  $\text{AlCu}$  IMC layers.

By increasing the annealing time to 6 days at 523 K (250 °C), obvious three IMC layers could be observed at the interface, and all the IMC grains exhibited an equiaxed shape, as shown in Figure 4(b). The three IMC layers were identified as  $\text{Al}_2\text{Cu}$ ,  $\text{AlCu}$ , and  $\text{Al}_4\text{Cu}_9$ , respectively, from the SAD analysis and the EDS results. Both the  $\text{Al}_2\text{Cu}$  and  $\text{AlCu}$  IMC layers exhibited constant composition which agreed well with their chemical formulas according to the EDS analysis (Figure 4(c)). However, the composition of the  $\text{Al}_4\text{Cu}_9$  IMC layer showed a transitional distribution of Al and Cu elements, and excessive Al existed in this IMC layer compared to that in the chemical formula. Besides, an obvious Cu-based solution layer with the Al solution concentration as high as 20 at. pct was observed between the  $\text{Al}_4\text{Cu}_9$  IMC layer and the Cu bulk from the EDS analysis (Figure 4(c)). The typical SAD pattern of the Cu-based solution is shown in Figure 4(d), which exhibited a modulated structure. In addition to the primary strong spots which diffracted from the  $[-122]$  zone axis of Cu, some relatively weak spots could be also observed, and these should be related to the high concentration of solute Al atoms.

Figure 5 shows the detailed microstructure and the EPMA analysis results of the Al-Cu interface after annealing for 10 hours at 673 K (400 °C). Three IMC

layers with different element contents could be observed at the Al-Cu interface (Figure 5(b)), which were  $\text{Al}_2\text{Cu}$ ,  $\text{AlCu}$ , and  $\text{Al}_4\text{Cu}_9$  IMC layers from the Al side to the Cu side, respectively. Similar to the EDS results from TEM, the compositions of  $\text{Al}_2\text{Cu}$  and  $\text{AlCu}$  IMC layers were relatively constant, and the  $\text{Al}_4\text{Cu}_9$  layer exhibited a transitional composition distribution, as shown in Figure 5(c).

### C. Growth Behavior of the IMCs at the Interface

In general, the solid-state growth of the IMCs can follow linear or parabolic growth kinetics, which are controlled by the reaction rate at the growth site and volume diffusion, respectively.<sup>[4,11–13]</sup> Figure 6 shows the dependence of the square of the interfacial IMC thickness on the annealing time. It can be clearly seen from Figure 6(a) that the square of the total IMC thickness increased linearly with the annealing time at 523 K (250 °C), which suggested that the growth of the IMC layer followed parabolic growth kinetics. In this case, the growth behavior of the IMC layer can be expressed by the following equation:

$$d^2 = kt, \quad [1]$$

where  $d$  is the thickness of the IMC layer,  $k$  is the growth rate constant, and  $t$  is the annealing time. Therefore, the

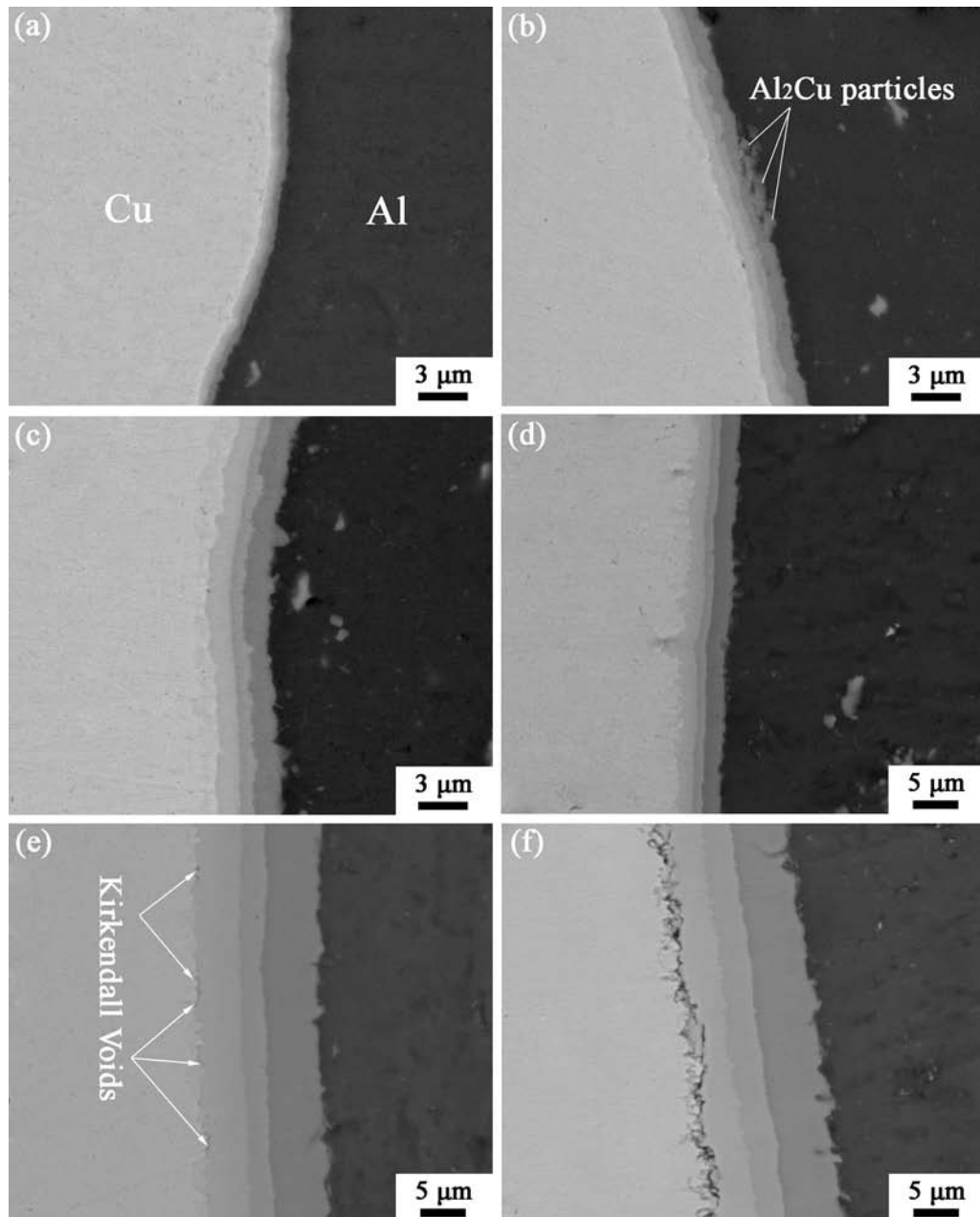


Fig. 3—SEM micrographs showing interface development of Al-Cu joints under various annealing conditions: at 523 K (250 °C) for (a) 1 day, (b) 3 days, (c) 6 days, and at 673 K (400 °C) for (d) 1 h, (e) 9 h, (f) 11 h.

$k$  value decided the growth rate of the IMC layer, and it can be calculated from the linear regression analysis of  $d^2$  vs  $t$ , where the slope is equal to the  $k$  value. The  $k$  value was calculated to be  $1.16 \times 10^{-17} \text{ m}^2/\text{s}$  for the annealing process of the FSW Al-Cu joints at 523 K (250 °C), as shown in Table I.

Similarly, parabolic growth behavior of the total IMC layer was also observed when the joints were annealed at 673 K (400 °C) till 9 hours; however, the growth rate of the IMC layer reduced after 9 hours (Figure 6(b)). The growth kinetics of each IMC layer annealed at 673 K (400 °C) was also investigated in this study, as shown

in Figures 6(c) and (d). Clearly, the  $\text{Al}_2\text{Cu}$  and  $\text{Al}_4\text{Cu}_9$  IMC layers both exhibited parabolic growth behaviors (Figure 6(c)). Similar to the total IMC layer, the growth rates of the  $\text{Al}_2\text{Cu}$  and  $\text{Al}_4\text{Cu}_9$  IMC layers, *i.e.*, the  $k$  values, were reduced and even minus after annealed for more than 9 hours. For the AlCu IMC layer, however, the parabolic growth behavior could be observed till the longest annealing time of 11 hours in this study. The growth rate constants calculated from the linear parts for the total and single IMC layers annealed at 673 K (400 °C) are shown in Table I.

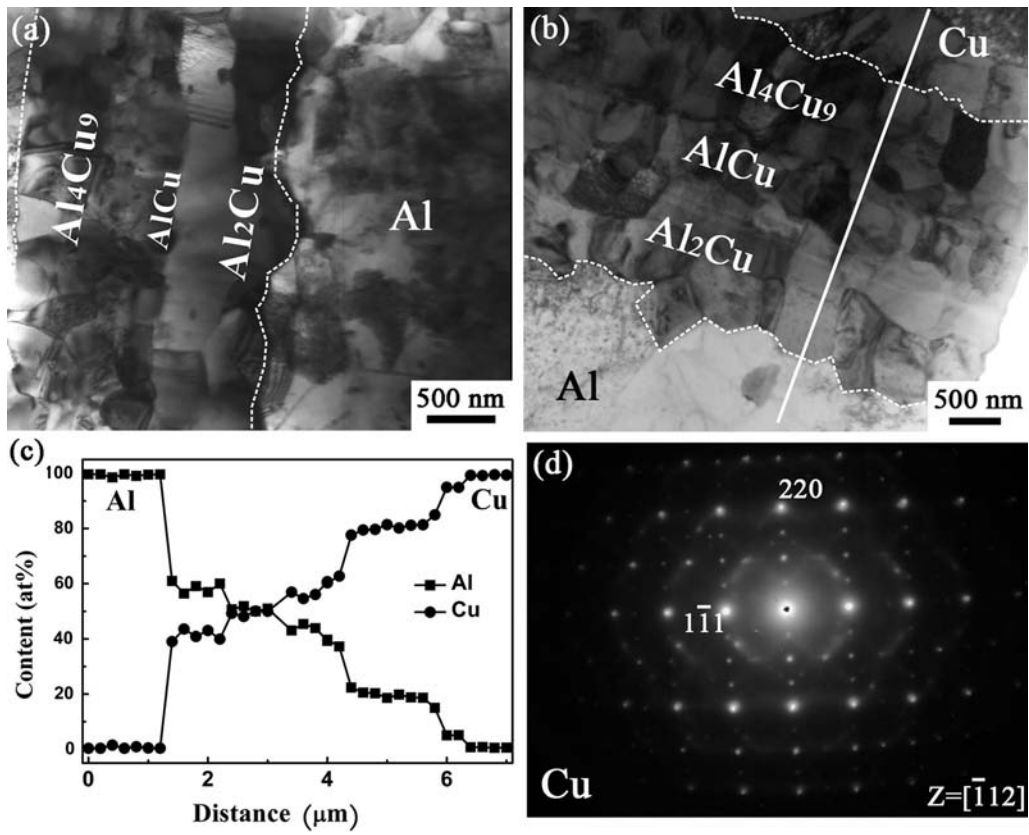


Fig. 4—TEM images showing interfacial microstructures after annealed at 523 K (250 °C) for (a) 3 days, (b) 6 days, and (c) EDS line analysis perpendicular to the interface along the line schematically shown in (b), (d) typical SAD pattern of Cu solution layer.

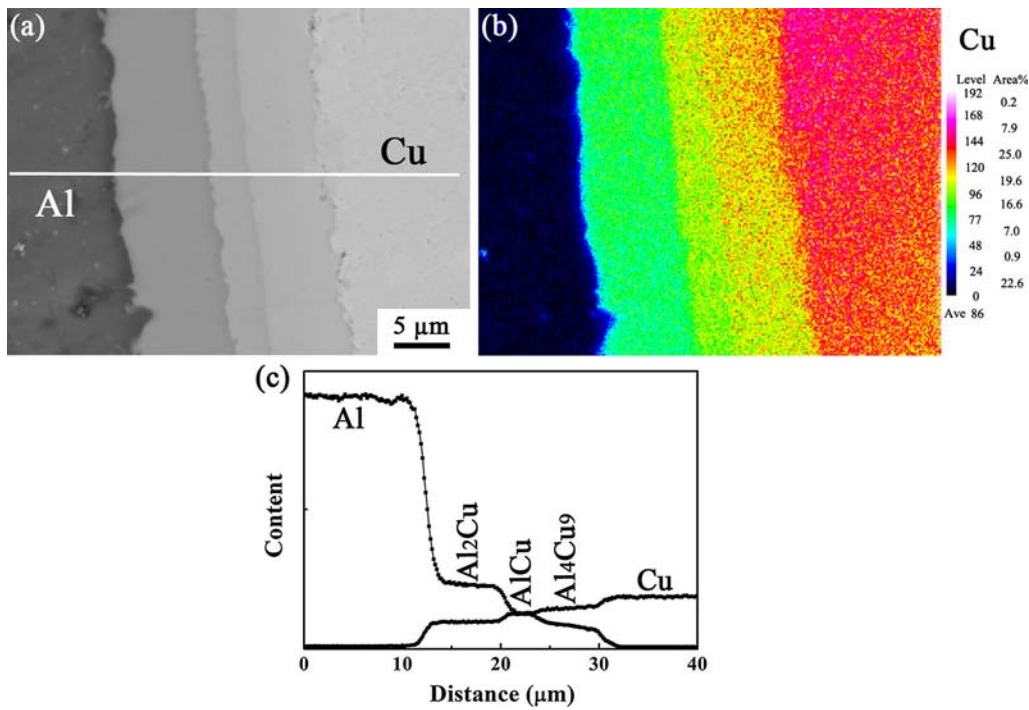


Fig. 5—(a) SEM microstructure and (b) EPMA element distribution map of the Al-Cu interface, and (c) EPMA line analysis perpendicular to the interface along the line schematically shown in (a).

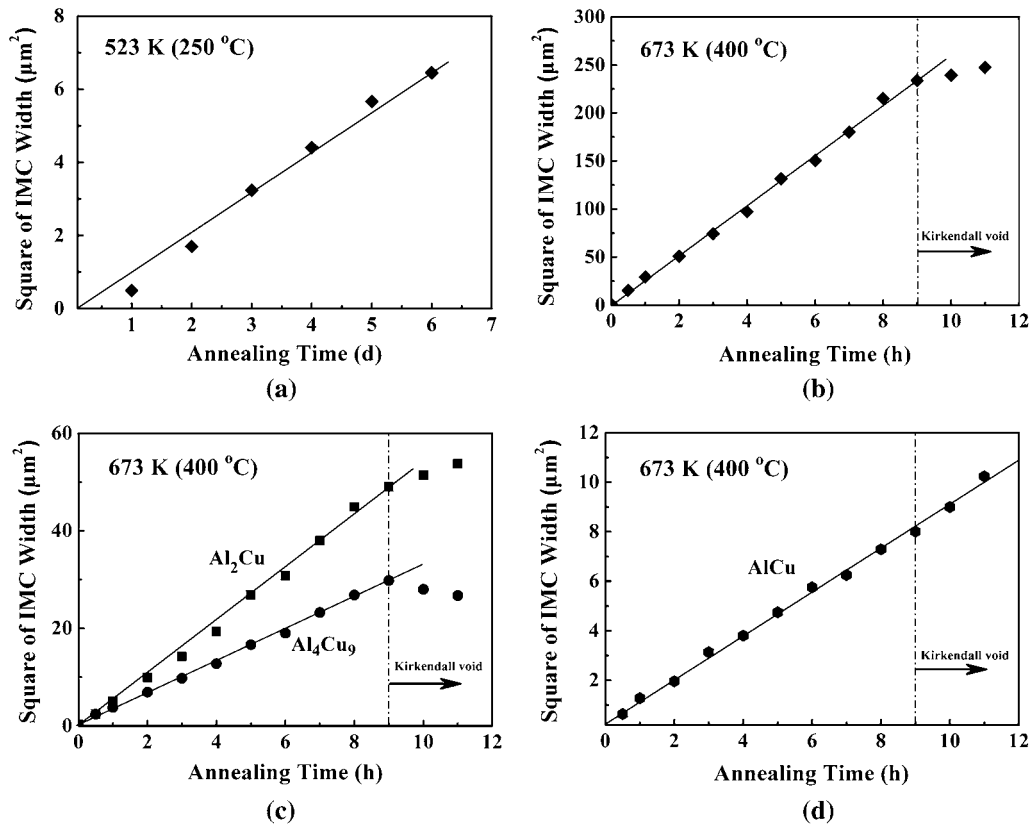


Fig. 6—Variation of square of interfacial IMC thickness with annealing time at various temperatures: total IMC layer at (a) 523 K (250 °C) and (b) 673 K (400 °C); (c) Al<sub>2</sub>Cu and Al<sub>4</sub>Cu<sub>9</sub> layers, and (d) AlCu layer at 673 K (400 °C).

Table I. Calculated Growth Rate Constants of the IMCs for Al-Cu Joints Prepared by FSW and Other Joining Methods

Temperature [K (°C)]	IMC	$k$ (m <sup>2</sup> /s)	Joining Methods
523 (250)	total	$1.17 \times 10^{-17}$	FSW (this study)
		$1.60 \times 10^{-17}$	FW <sup>[11]</sup>
		$6.30 \times 10^{-18}$	CRW <sup>[13]</sup>
673 (400)	total	$7.24 \times 10^{-15}$	FSW (this study)
		$3.00 \times 10^{-15}$	FW <sup>[11]</sup>
		$1.09 \times 10^{-14}$	CRW <sup>[13]</sup>
673 (400)	Al <sub>2</sub> Cu	$1.53 \times 10^{-15}$	FSW (this study)
		$8.51 \times 10^{-16}$	CRW <sup>[13]</sup>
673 (400)	AlCu	$7.24 \times 10^{-15}$	FSW (this study)
		$1.15 \times 10^{-15}$	CRW <sup>[13]</sup>
673 (400)	Al <sub>4</sub> Cu <sub>9</sub>	$9.05 \times 10^{-16}$	FSW (this study)
		$2.20 \times 10^{-15}$	CRW <sup>[13]</sup>

#### D. Mechanical Properties of the Al-Cu Joints After Annealing

Figure 7 shows the relationship between the IMC thickness and the tensile strength of the FSW Al-Cu joints. It can be seen that the ultimate tensile strength (UTS) was closely related to the IMC thickness. When annealed at 523 K (250 °C), the joint fractured at the heat-affected zone (HAZ) of the Al side when the thickness of the IMC layer was smaller than ~2.5 μm. Meanwhile, the UTS decreased gradually with increasing the annealing time, which was due to the annealing softening effect in the HAZ. The FSW joints fractured at the Al-Cu interface when the IMC layer was thicker

than 2.5 μm [annealed for more than 3 days at 523 K (250 °C)], and the UTS decreased to ~90 MPa. When annealed at 673 K (400 °C) for half an hour, the Al-Cu joint with an IMC layer thickness of ~2.5 μm fractured at the HAZ, but the UTS decreased to ~80 MPa due to the strong annealing softening effect at the high temperature. Because of the enhanced growth rate of the IMC layer annealed at 673 K (400 °C), the joints fractured at the Al-Cu interface when the annealing time was longer than an hour. In this case, the UTS fluctuated between ~50 and ~60 MPa.

Figure 8 shows the typical microstructure of the fracture surfaces when the FSW joints failed at the



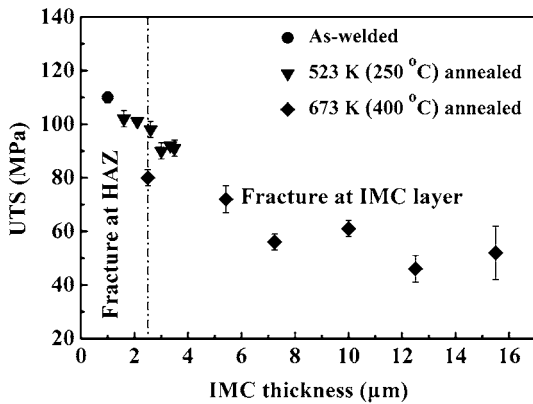


Fig. 7—Variation of UTS with thickness of total IMC layers.

Al-Cu interface, *i.e.*, in the IMC layers. Although the morphology of the fracture surfaces all exhibited brittle mode, there were always two types of fracture characteristics. When annealed at 523 K (250 °C) for 3-6 days and 673 K (400 °C) for less than 2 hours, *i.e.*, the thickness of the IMC layer was relatively small, the inter-granular fracture feature could be clearly observed from the fracture surfaces at both Cu side and Al side, as shown in Figures 8(a) and (b). The IMC grains exhibited equiaxed shape at both fracture surfaces, which was consistent with the morphology of the grains observed by TEM (Figure 4(b)). Furthermore, the IMC grains were umbilicate at the Al side and protuberant at the Cu side. EDS analysis results indicated that the element compositions of the IMC grains were close to  $\text{Al}_2\text{Cu}$  and  $\text{AlCu}$  IMCs at the Al side and Cu side, respectively.

As the thickness of the IMC layer increased, trans-granular fracture characteristic gradually developed. Figure 8(c) shows a typical transition zone of the inter-granular fracture and trans-granular fracture for the Al-Cu joints annealed for 5 hours at 673 K (400 °C). When the IMC layer thickness increased further, trans-granular fracture became the major fracture mode, as shown in Figure 8(d). Certainly, at a very high annealing temperature and/or long annealing time, the Al-Cu joints failed at the interface between the Cu BM and the IMC layers due to the formation of the Kirkendall tunnel.

Figure 9 shows the XRD patterns of the fracture surfaces after tensile testes at the Cu side and Al side for the samples annealed at 523 K (250 °C). It is clear the characteristic diffraction peaks of the  $\text{Al}_4\text{Cu}_9$  and  $\text{AlCu}$  IMCs were detected at the Cu sides for the samples annealed for 3 and 6 days at 523 K (250 °C). No obvious diffraction peaks of the  $\text{Al}_2\text{Cu}$  phase were found at the Cu side. However, XRD analysis at the Al side revealed the distinct characteristic diffraction peaks of  $\text{Al}_2\text{Cu}$ . Moreover, weak characteristic diffraction peaks of Cu and  $\text{Al}_4\text{Cu}_9$  could also be detected, which may be due to the reaction between the Cu particles and the Al BM in the NZ.<sup>[22]</sup>

Figures 10(a) and (b) show the side views of the failed FSW Al-Cu joints annealed for 3 days at 523 K (250 °C) and for 10 hours at 673 K (400 °C), respectively. As shown in Figure 10(a), the joint failed at the Al-Cu

interface. From the magnified image of Al side (shown by the rectangle), it is clear that only one IMC layer of  $\text{Al}_2\text{Cu}$  remained at the Al side of the failed sample, indicating that the joint fractured mainly along the boundary between the  $\text{Al}_2\text{Cu}$  and the  $\text{AlCu}$  IMC layers. Furthermore, around the larger Cu pieces in the NZ, three IMC layers could also be observed. Similarly, crack initiated along the boundary of the  $\text{Al}_2\text{Cu}$  and  $\text{AlCu}$  IMC layers. Simultaneously, few  $\text{Al}_2\text{Cu}$  would be detached from the Al base during tension, as shown by the arrow in the bottom (Figure 10(a)). When the IMC layer was very thick, the joint also failed at the interface as shown in Figure 10(b). However, no regular fracture feature was found in this case. As cracks could develop through all the three IMC layers or along their boundaries, all the three IMC layers could be observed on both fracture surfaces of the failed samples (Figure 10(b)).

## IV. DISCUSSION

### A. Microstructure Evolution During FSW

During the FSW process, the material underwent intense plastic deformation at elevated temperature, resulting in dynamic recrystallization.<sup>[18,31]</sup> For the dissimilar joints, however, the material flow is more complex especially at the bonding interface.<sup>[19]</sup> In the present Al-Cu system, for example, the material flow took place mainly in the Al matrix because the pin offset was performed.<sup>[22]</sup> In other words, the Cu BM at the border of the NZ hardly deformed during FSW, and the Al matrix should deform more severely near the border than that in the NZ. Meanwhile, enhanced Al-Cu interdiffusion took place under the elevated temperature and the severe deformation during FSW. In the Al-Cu diffusion system, there is a greater diffusivity of Cu in Al than that of Al in Cu.<sup>[16,32]</sup> In this case, a supersaturated  $\alpha$ -Al layer with high density of dislocations would form easily between the Cu BM and the Al matrix of the NZ.

The formation of the Al-Cu IMCs is thermally activated, and the development of the interfacial phase is affected by their formation energies. Previous studies indicated that  $\text{Al}_2\text{Cu}$  and  $\text{Al}_4\text{Cu}_9$  were the first two IMC phases formed at the Al-Cu interface.<sup>[14,15,33]</sup> In a study of phase development for the Al-Cu system, Jiang *et al.*<sup>[33]</sup> reported that the formation energies of  $\text{Al}_2\text{Cu}$  and  $\text{Al}_4\text{Cu}_9$  phases were 0.78 and 0.83 eV, respectively. Because Cu diffuses faster than Al and the solid solubility of Cu in Al is very low (~0.33 at. pct), the Al side is the first to reach the maximum supersaturated concentration near the interdiffusion interface.

Furthermore, because of the existence of high density of dislocations in the  $\alpha$ -Al layer, the diffusion of the Cu atoms to the  $\alpha$ -Al layer was easier due to the short-circuit diffusion. And thus, the  $\text{Al}_2\text{Cu}$  phase would first form mainly by the means of consuming the  $\alpha$ -Al layer. Because the diffusion rate of the Cu atoms is almost identical in the whole  $\alpha$ -Al layer, columnar grains would form easily, as shown in Figures 1(c) and 2(b). Similarly, columnar  $\text{Al}_2\text{Cu}$  grains were also observed at the



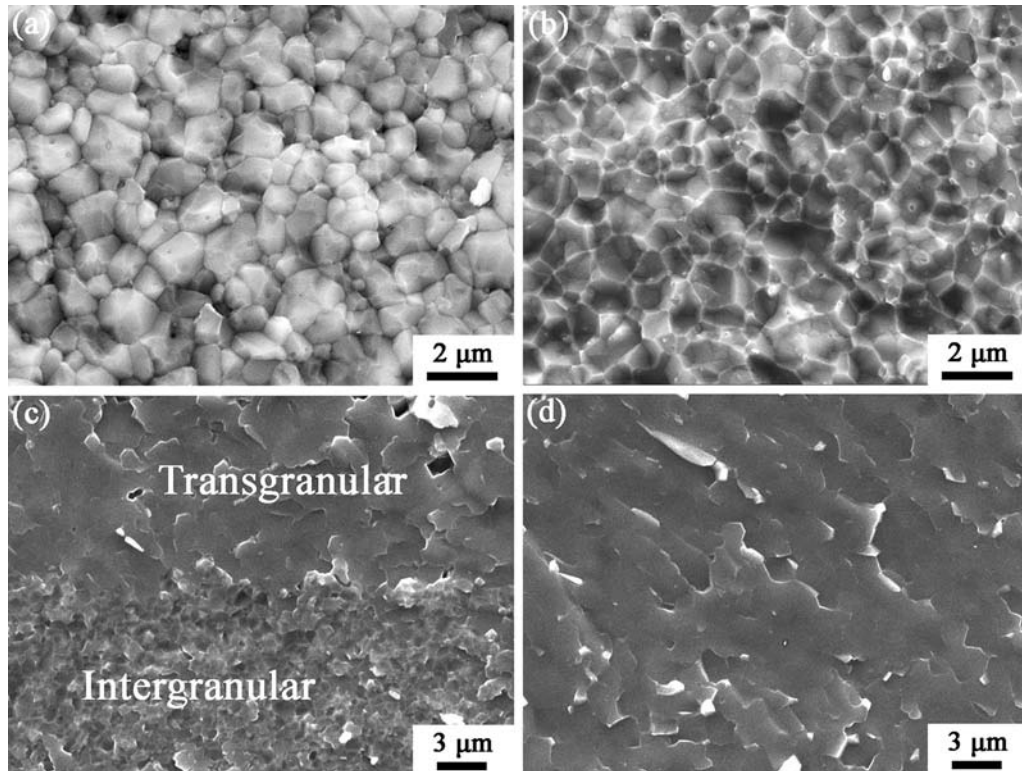


Fig. 8—SEM fractographs of FSW Al-Cu joints after annealed for 5 days at 523 K (250 °C) of (a) Cu side, (b) Al side, and (c), (d) 5 h at 673 K (400 °C) of Al side.

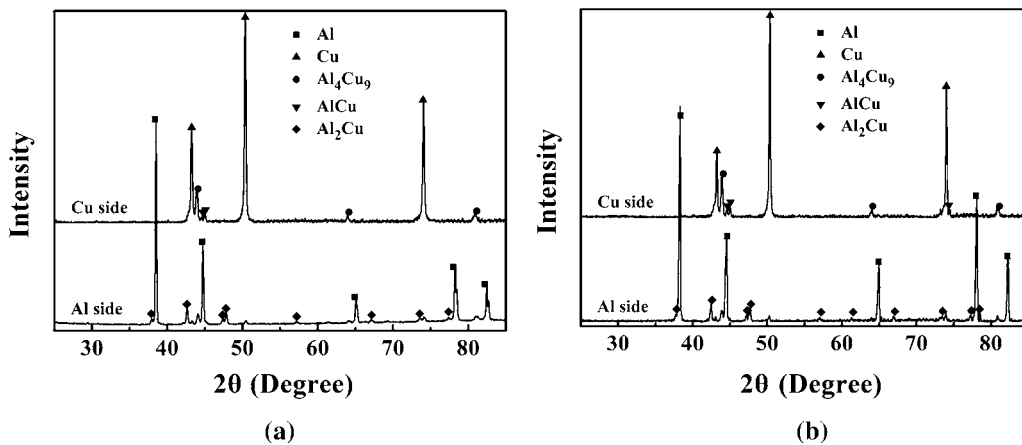


Fig. 9—XRD patterns measured on the tensile fracture surfaces for FSW Al-Cu joints annealed at 523 K (250 °C) for (a) 3 days and (b) 6 days.

interface of FSW dissimilar Al-Cu joints in other studies.<sup>[23,24]</sup>

During the growth process of the  $\text{Al}_2\text{Cu}$  phase, the diffusion rates of the Cu atoms would be different along the various lattice planes in the  $\text{Al}_2\text{Cu}$  grains.<sup>[5,13,32]</sup> Then, the sizes of the  $\text{Al}_2\text{Cu}$  grains would be different in layer B (Figure 1(c)), and the thickness of the remnant  $\alpha$ -Al layer became different and even discontinuous. On the other hand, more and more Al atoms would diffuse to the Cu BM with the formation and growth of the  $\text{Al}_2\text{Cu}$ , and new  $\text{Al}_4\text{Cu}_9$  grains formed at the Cu side when the appropriate concentration was reached. The lattice diffusion rates were different along the various

crystal planes of the Cu BM and  $\text{Al}_2\text{Cu}$  grains. So the  $\text{Al}_4\text{Cu}_9$  grains with an irregular shape formed between the  $\text{Al}_2\text{Cu}$  layer and the Cu BM. The  $\text{Al}_2\text{Cu}$  and  $\text{Al}_4\text{Cu}_9$  grains grew gradually with the development of the interdiffusion, resulting in the formation of two distinct IMC layers.

Meanwhile, the nucleation requirement of the AlCu phase would be satisfied between the  $\text{Al}_2\text{Cu}$  and  $\text{Al}_4\text{Cu}_9$  layers, and few fine AlCu IMC grains nucleated and grew. In other words, AlCu IMC was developed by consuming  $\text{Al}_2\text{Cu}$  and/or  $\text{Al}_4\text{Cu}_9$  phases. Usually, an orthorhombic AlCu phase is hard to nucleate on a tetragonal  $\text{Al}_2\text{Cu}$  phase, but preferentially on a cubic

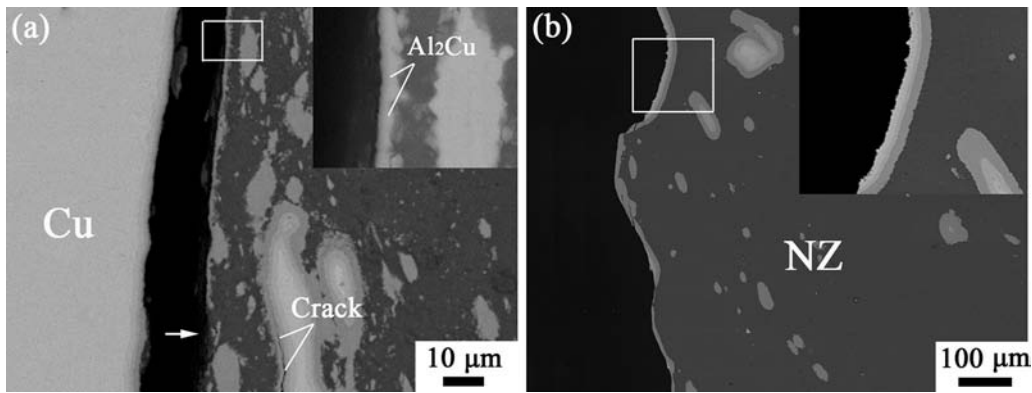


Fig. 10—Cross-section images (BEI) of the fractured FSW Al-Cu joints annealed for (a) 3 days at 523 K (250 °C), and (b) 10 h at 673 K (400 °C).

$\text{Al}_4\text{Cu}_9$  phase. Excessive solute Al atoms usually exist in  $\text{Al}_4\text{Cu}_9$ ,<sup>[34–36]</sup> which is beneficial to the nucleation of  $\text{AlCu}$ . Therefore, the  $\text{AlCu}$  phases preferentially nucleate and grow by consuming the  $\text{Al}_4\text{Cu}_9$  phases in layer C, and layer B still keeps its columnar morphology (Figure 2(d)). This should be the reason why layer C at the interface was consisted of  $\text{AlCu}$  and  $\text{Al}_4\text{Cu}_9$  phases, but only  $\text{Al}_2\text{Cu}$  phase was observed in layer B.

#### B. Development and Growth Kinetic of the IMCs During Annealing

From the present observations as well as the previous studies,<sup>[4,5,11–17]</sup> it is clear that complex structural transformation occurred at the Al-Cu interface during annealing process. After annealing, the  $\alpha$ -Al layer (layer A) with high density of dislocations disappeared. This indicated that the growth of  $\text{Al}_2\text{Cu}$  consumed the whole  $\alpha$ -Al layer. Because of the disappearance of the  $\alpha$ -Al layer, the interdiffusion rates of the Cu atoms and Al atoms would be different in the  $\text{Al}_2\text{Cu}$  grains. Furthermore, new  $\text{Al}_2\text{Cu}$  grains would nucleate and grow at the boundaries of the columnar grains due to the high energy state and the high diffusion rate. The columnar grains could not keep their original morphology in this case, and then developed into equiaxed grains gradually during the annealing process. With the development of the annealing process, more and more  $\text{Al}_2\text{Cu}$  grains nucleated and grew, while the former equiaxed grains kept on growing. Therefore, the original single layer of columnar  $\text{Al}_2\text{Cu}$  grains was replaced by a new layer with many equiaxed  $\text{Al}_2\text{Cu}$  grains, as shown in Figures 4(a) and (b). Similarly, equiaxed  $\text{Al}_4\text{Cu}_9$  grains nucleated and grew with the development of interdiffusion during the annealing process.

At the same time, more and more  $\text{AlCu}$  grains nucleated and grew in the  $\text{Al}_4\text{Cu}_9$  layer or between the  $\text{Al}_2\text{Cu}$  layer and  $\text{Al}_4\text{Cu}_9$  layer. The  $\text{AlCu}$  grains connected with each other and a new IMC layer would form when the number of the  $\text{AlCu}$  grains was large enough. So, three distinct IMC layers could be observed (Figure 3).

In the binary diffusion couple, the inequality of intrinsic diffusion coefficients usually results in a

movement of inert markers, or lattice drift, known as the Kirkendall effect.<sup>[37]</sup> Following the scenario of Smigelkas and Kirkendall,<sup>[38]</sup> pores occur on the side of the faster diffusing element (Cu in this case<sup>[16,32]</sup>), where vacancies move in the opposite direction of the dominant diffusive flux and condense into Kirkendall voids.<sup>[2]</sup> In the present study, the non-equilibrium diffusivity between Al and Cu promoted the Kirkendall effect of void formation, and the Kirkendall voids were observed to gather at the boundaries between the Cu-rich IMC layers and the Cu BM after prolonged annealing, resulting in the formation of Kirkendall tunnel.<sup>[10–16]</sup>

The growth kinetics of the IMCs is very important for the Al-Cu joints in practical application, because the joints tend to fail when the IMC layer is too thick. As shown in the present results, the growth of the Al-Cu IMCs was controlled by the volume diffusion, and could be expressed by Eq. [1]. Then, the  $k$  value in Eq. [1] decided the growth rate of the IMCs. Table I shows the calculated growth rate constants of the IMCs for the Al-Cu joints prepared by FSW, FW, and CRW.<sup>[11,13]</sup> It is clear that at 523 K (250 °C), the growth kinetics of the total IMC layers was relatively low. However, at 673 K (400 °C), the rate of the total and each IMC growth was quite appreciable.

At 523 K (250 °C), the  $k$  value of FSW joints was similar to that of FW joints but higher than that of CRW joints, indicating that the IMC growth rate of CRW joint was lower than that of FW and FSW joints. Usually, an IMC layer had pre-existed in the FSW and FW joints, but no obvious IMC formation was observed in the initial CRW joints.<sup>[5,12,13,16]</sup> It would take more time to form the new IMC layer first for the CRW joints, which reduced the growth rate. At a higher temperature of 673 K (400 °C), however, the new IMC layer was very easy to form. Therefore, the total IMC growth rate in the CRW joints would be similar to that in the FW and FSW joints. In this case, a slightly higher  $k$  value was obtained for the CRW joints (Table I).

It should be emphasized that the growth kinetics of the IMCs were greatly influenced by the Kirkendall effect at higher annealing temperature and/or longer annealing time. It is well accepted that the diffusion of

Cu atoms would be restricted when the Kirkendall voids were formed at the interface between  $\text{Al}_4\text{Cu}_9$  and Cu BM, resulting in the decreased diffusion rate of Cu atoms.<sup>[2,16,32,37,38]</sup> Therefore, the  $k$  values of the IMC layers were reduced after annealed for more than 9 hours at 673 K (400 °C), especially for the Cu-rich  $\text{Al}_4\text{Cu}_9$  layer where even minus  $k$  value was achieved (Figures 6(b) and (c)). However, for the AlCu layer, sufficient Cu atoms can be obtained from the Cu-rich  $\text{Al}_4\text{Cu}_9$  layer, resulting in the constant  $k$  value (Figure 6(d)).

Usually, a simple Arrhenius relationship was used to determine the activation energies for the IMC growth<sup>[4,5,11,13]</sup>:

$$k = k_0 \exp(-Q/RT), \quad [2]$$

where  $k_0$  is the frequency factor,  $Q$  is the activation energy,  $R$  is the gas constant (8.314 J/mol K), and  $T$  is the annealing temperature. The activation energy can be calculated from the slope of the Arrhenius plot. Figure 11 shows the Arrhenius relationship between the growth rate constants  $k$  and temperature  $T$  for the Al-Cu joints prepared by FSW and other joining methods.<sup>[11-13]</sup> It is clear that a strong linear Arrhenius relationship can be observed for all the data from various joining methods, with unified activation energy being determined to be 117 kJ/mol. This indicates that the IMC growth kinetic of the Al-Cu joints prepared by FSW was similar to that by other solid-state welding methods, and no accelerated growth phenomenon was observed in the FSW joints.

### C. Mechanical Properties and Fracture Behavior

The present results showed that the mechanical properties of Al-Cu joints were strongly affected by the IMC layers at the interface. Previous study indicated that the Al-Cu joints rapidly lose their mechanical integrity when the thickness of the IMC layer reached a critical value of  $\sim 2 \mu\text{m}$ .<sup>[14]</sup> Similarly, a critical IMC thickness of  $\sim 2.5 \mu\text{m}$  was also observed in the present study, which is consistent with the result of Abbasi *et al.*<sup>[12]</sup>

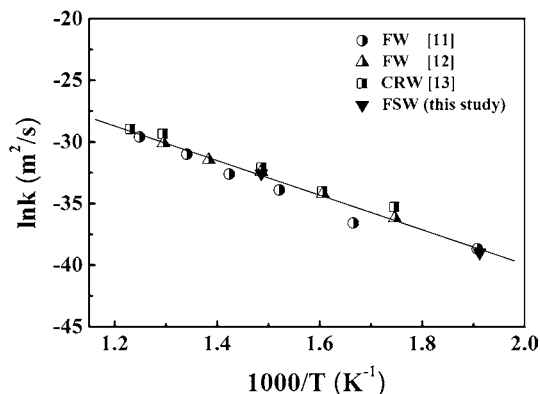


Fig. 11—Arrhenius plot for the growth rate of total IMC layers for Al-Cu joints prepared by FSW and other welding methods.<sup>[11-13]</sup>

When the IMC layer was slightly thicker than  $2.5 \mu\text{m}$  after annealed at 523 K (250 °C), the joints began to fracture at the interface and the UTS decreased to about 90 MPa, which was a little lower than that of the joints fractured at the HAZ of the Al side ( $\sim 100$  MPa). In a study of CRW Al-Cu joints, Abbasi *et al.*<sup>[12]</sup> indicated that the strength decreased clearly once the thickness of the IMC layer exceeded the critical value. In the present study, relatively high UTS of  $\sim 50$  MPa could be obtained even if the thickness of the IMC layer was very large after annealed at 673 K (400 °C). This suggests that the reliable FSW joints could be still obtained when the thickness of the IMC layer was larger than the critical value.

In the present study, it is clear that the fracture behavior of the annealed FSW Al-Cu joints was influenced by the IMCs obviously, as shown schematically in Figure 12. When the thickness of the IMC layer was larger than  $2.5 \mu\text{m}$ , the IMC layer would increase the brittleness of the interface, leading to easier crack initiation and propagation. Nakamura *et al.*<sup>[15]</sup> suggested that the  $\theta$  phase ( $\text{Al}_2\text{Cu}$ ) was the weakest IMC at the Al-Cu interface. If a thick  $\theta$  phase film formed over the entire interface, the ductility of the joint would deteriorate. Other researchers indicated that the fracture did not occur in a single IMC layer but through the whole IMC layers.<sup>[5,13,15]</sup> For the present FSW Al-Cu joints, however, the fracture behavior changed with the thicknesses of the IMC layer.

When the thickness of the IMC layer was relatively small, for example, the samples annealed at 523 K and 673 K (250 °C and 400 °C) for 1 hour in this study, the joints failed mainly along the boundary of the  $\text{Al}_2\text{Cu}$  and AlCu IMC layers (Figures 8(a), (b) and 9). Wallach and Davies<sup>[14]</sup> also suggested that the fracture developed between the  $\text{Al}_2\text{Cu}$  and AlCu phases under the thick IMC layer up to  $25 \mu\text{m}$ , but the convincing evidences and mechanism analysis were lacking. It is reasonable to expect that the crack initiation is difficult to take place between the BM and the IMCs due to the existence of the ductile BM. Therefore, the interface between different IMC layers would be the weakest regions in the whole interfacial layers. As mentioned before, AlCu first nucleated and grew in the  $\text{Al}_4\text{Cu}_9$  IMC layers, where excess Al atoms existed. This indicated that the bonding strength between AlCu and  $\text{Al}_4\text{Cu}_9$  phases would be

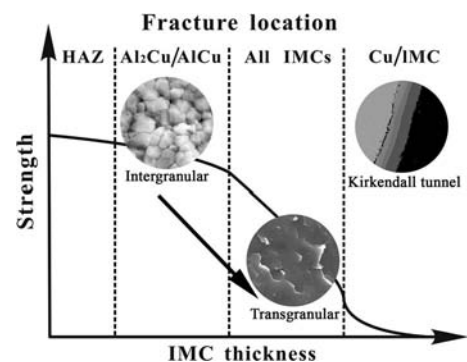


Fig. 12—Schematic diagram showing relationship between strength, fracture location, and IMC thickness of FSW Al-Cu joints.



higher than that between AlCu and Al<sub>2</sub>Cu phases. In this case, the crack mainly propagated along the interface between AlCu and Al<sub>2</sub>Cu IMC layers, and the inter-granular fracture occurred (Figures 8(a) and (b)).

After annealing for 5 hours at 673 K (400 °C) in this study (the thickness of the IMC layer was ~10 μm), the fracture behavior was complex. Fracture mechanism began to transform from inter-granular to trans-granular, as shown in Figure 8(c). As the annealing time increased, trans-granular became the main fracture mode, and the crack propagated at the whole IMC layers according to the SEM result (Figure 10(b)). It is well known that the Al-Cu IMCs are brittle phases due to their non-metallic covalence bond.<sup>[4,12]</sup> When the thickness of the IMC layer at the interface was small, crack initiation in the narrow space of the IMC layer was very difficult. Then favorable bonding strength could be obtained in this case. However, when the IMC layer was very thick, the brittleness of the IMCs would exhibit obviously. The whole IMC became brittle, and the crack was easy to propagate in any IMC layer of the interface. So, irregular crack propagation and trans-granular fracture were usually observed.<sup>[14]</sup>

Under enough long annealing time and/or higher annealing temperature, the non-equilibrium interdiffusion between Al and Cu promotes the Kirkendall effect of void formation, and the Kirkendall voids gathered at the boundary between the Al<sub>4</sub>Cu<sub>9</sub> IMC layer and the Cu BM (Figures 3(e) and (f)). The Kirkendall voids were also found at the boundaries between the Cu-rich IMC layer and Cu BM in other studies, which would affect the mechanical properties of the Al-Cu joints.<sup>[10–16]</sup> It is widely accepted that crack initiation and propagation easily occurred along the Kirkendall voids especially when they connected into Kirkendall tunnel, resulting in very low bonding strength. Moreover, it is found that when annealed at very long time and/or very high temperature in this study, the samples of Al-Cu joints already fractured along the Kirkendall tunnel.

It can be concluded that the strength of the FSW Al-Cu joints is controlled by the thickness of the IMC layers at the interface. At a smaller thickness of less than 2.5 μm, sound metallurgical bonding can be achieved between the IMCs and BM, resulting in the high UTS of ~100 MPa with the fracture occurring at the HAZ of the Al side. When the IMC layer became thicker, the joints fractured at the interface, and the UTS decreased from ~90 to 50–60 MPa as the thickness increased, together with the fracture mode changing from inter-granular to trans-granular. When the Kirkendall voids connected into a tunnel after very long annealing time and/or very high temperature, the joints fractured along the Kirkendall tunnel with very low strength.

## V. CONCLUSIONS

The present study investigated the evolution of the IMC layer at the interface of FSW Al-Cu joints under both the as-welded and annealed states, and the relationship between the thickness of the IMC layer and

mechanical properties was analyzed. The following conclusions can be drawn:

1. In the as-FSW Al-Cu joints, an obvious interface ~1 μm in thickness, which was composed of three sub-layers, was observed between the Cu BM and the NZ. The first layer near the Al matrix was discontinuous and determined to be α-Al supersaturated solid solution layer with high density of dislocations. The second layer near the α-Al layer was Al<sub>2</sub>Cu IMCs with columnar grains. In the third layer near the Cu BM most grains were Al<sub>4</sub>Cu<sub>9</sub> with an irregular shape, and few fine AlCu IMC grains were also observed.
2. As the annealing time and/or temperature increased, the interface continued thickening and developing into three IMC layers. The initial α-Al layer was gradually consumed during the growth process of Al<sub>2</sub>Cu IMC, and the columnar grains were replaced by equiaxed grains in the Al<sub>2</sub>Cu layer with the development of annealing process. At the same time, more and more equiaxed grains generated in the Al<sub>4</sub>Cu<sub>9</sub> layer. Moreover, a new continuous IMC layer with equiaxed AlCu grains developed between the Al<sub>2</sub>Cu and Al<sub>4</sub>Cu<sub>9</sub> IMC layers. Accompanied with the growth of IMC layers, Kirkendall voids gradually formed at the boundary between Cu BM and Al<sub>4</sub>Cu<sub>9</sub> IMC layer, and connected together into the Kirkendall tunnels.
3. The growth of the IMC layers can be described by the parabolic rate laws before the formation of the Kirkendall voids. Reduced and even minus growth rates were achieved in the Al<sub>2</sub>Cu and Al<sub>4</sub>Cu<sub>9</sub> IMC layers after the formation of the Kirkendall voids, but the AlCu IMC layer exhibited parabolic growth behavior during the whole annealing process. By combining the growth rate constants from the present work and previous studies, an activation energy of 117 kJ/mol can be obtained for the whole IMC layer growth in Al-Cu joints from an Arrhenius plot.
4. The strength of the FSW Al-Cu joints was controlled by the thickness of the IMC layers at the interface. At a smaller thickness of less than 2.5 μm, sound metallurgical bonding could be achieved between the IMC and BM, resulting in the high UTS of ~100 MPa with the fracture occurring at the HAZ of the Al side. When the IMC layer became thicker, the joints fractured at the interface, and the UTS decreased from ~90 to 50–60 MPa as the thickness increased.
5. Different fracture modes were observed when the FSW Al-Cu joints fractured at the interface. At a relatively smaller thickness of IMC layer, the cracks propagated along the boundary of Al<sub>2</sub>Cu and AlCu IMC layers, and the inter-granular fracture was predominant. However, the cracks propagated in the whole IMC layers with a large thickness, and the trans-granular fracture occurred. The Al-Cu joints would fracture along the Kirkendall tunnel with very low strength in the case of the formation of Kirkendall tunnels.

## ACKNOWLEDGMENTS

This work was supported by the National Natural Science Foundation of China under Grant No. 51331008.

## REFERENCES

1. M. Ghosh, R.K. Gupta, and M.M. Husain: *Metall. Mater. Trans. A*, 2014, vol. 45A, pp. 854–63.
2. H. Springer, A. Kostka, E.J. Payton, D. Raabe, A. Kaysser-Pyzalla, and G. Eggeler: *Acta Mater.*, 2011, vol. 59, pp. 1586–1600.
3. B. Gulenc: *Mater. Des.*, 2008, vol. 29, pp. 275–78.
4. W.B. Lee, K.S. Bang, and S.B. Jung: *J. Alloy Compd.*, 2005, vol. 390, pp. 212–19.
5. C.Y. Chen, H.L. Chen, and W.S. Hwang: *Mater. Trans.*, 2006, vol. 47, pp. 1232–39.
6. U.F.H. Suhuddin, V. Fischer, and J.F. dos Santos: *Scripta Mater.*, 2013, vol. 68, pp. 87–90.
7. M. Shakil, N.H. Tariq, M. Ahmad, M.A. Choudhary, J.I. Akhter, and S.S. Babu: *Mater. Des.*, 2014, vol. 55, pp. 263–73.
8. J. Kim and Y. Kawamura: *Scripta Mater.*, 2011, vol. 65, pp. 1033–36.
9. Z. Sun: *Int. J. Mater. Prod. Technol.*, 1995, vol. 10, pp. 16–26.
10. W.E. Veerkamp: *IEEE Trans.*, 1995, Paper No. PCIC-95-20, pp. 187–95.
11. M. Braunović and N. Aleksandrov: *Electrical Contacts, Proceedings of the Annual Holm Conference on Electrical Contacts*, 1993, pp. 261–68.
12. M. Abbasi, A.K. Taheri, and M.T. Salehi: *J. Alloy Compd.*, 2001, vol. 319, pp. 233–41.
13. C.Y. Chen and W.S. Hwang: *Mater. Trans.*, 2007, vol. 48, pp. 1938–47.
14. E.R. Wallach and G.J. Davies: *Met. Technol.*, 1977, vol. 4, pp. 183–90.
15. M. Nakamura, Y. Yonezawa, T. Nakanishi, and K. Kondo: *Wire J.*, 1977, vol. 10, pp. 71–78.
16. X.K. Peng, R. Wührer, G. Heness, and W.Y. Yeung: *J. Mater. Sci.*, 1999, vol. 34, pp. 2029–38.
17. G. Heness, R. Wührer, and W.Y. Yeung: *Mater. Sci. Eng. A*, 2008, vols. 483–484, pp. 740–42.
18. R.S. Mishra and Z.Y. Ma: *Mater. Sci. Eng. R*, 2005, vol. 50, pp. 1–78.
19. T. DebRoy and H.K.D.H. Bhadeshia: *Sci. Technol. Weld. Join.*, 2010, vol. 15, pp. 266–70.
20. Y.F. Sun, H. Fujii, N. Takai, and Y. Okitsu: *Mater. Des.*, 2013, vol. 47, pp. 350–57.
21. L.E. Murr, Y. Li, R.D. Flores, E.A. Trillo, and J.C. McClure: *Mater. Res. Innovat.*, 1998, vol. 2, pp. 150–63.
22. P. Xue, B.L. Xiao, D.R. Ni, and Z.Y. Ma: *Mater. Sci. Eng. A*, 2010, vol. 527, pp. 5723–27.
23. C.W. Tan, Z.G. Jiang, L.Q. Li, Y.B. Chen, and X.Y. Chen: *Mater. Des.*, 2013, vol. 51, pp. 466–73.
24. M.N. Avettand-Fenoël, R. Taillard, G. Ji, and D. Goran: *Metall. Mater. Trans. A*, 2012, vol. 46A, pp. 4655–66.
25. P. Liu, Q.Y. Shi, X.D. Wang, W. Wang, and X. Wang: *Mater. Lett.*, 2008, vol. 62, pp. 4106–08.
26. P. Xue, D.R. Ni, D. Wang, B.L. Xiao, and Z.Y. Ma: *Mater. Sci. Eng. A*, 2011, vol. 528, pp. 4683–89.
27. I. Galvão, A. Loureiro, D. Verdera, D. Gestó, and D.M. Rodrigues: *Metall. Mater. Trans. A*, 2012, vol. 43A, pp. 5096–5105.
28. J.H. Ouyang, E. Yarrapareddy, and R. Kovacevic: *J. Mater. Process. Technol.*, 2006, vol. 172, pp. 110–22.
29. ASM Handbooks: *Alloy Phase Diagrams*, ASM International, Materials Park, 2002, vol. 3.
30. G.V. Kidson: *J. Nucl. Mater.*, 1961, vol. 3, pp. 21–29.
31. T.R. McNelley, S. Swaminathan, and J.Q. Su: *Scripta Mater.*, 2008, vol. 58, pp. 349–54.
32. J. Askill: *Tracer Diffusion Data for Metals, Alloys, and Simple Oxides*, IFI Plenum, New York, 1970, p. 31.
33. H.G. Jiang, J.Y. Dai, H.Y. Tong, B.Z. Ding, Q.H. Song, and Z.Q. Hu: *J. Appl. Phys.*, 1993, vol. 74, pp. 6165–69.
34. Y.J. Guo, G.J. Qiao, W.Z. Jian, and X.H. Zhi: *Mater. Sci. Eng. A*, 2010, vol. 527, pp. 5234–40.
35. S. Westman: *Acta Chem. Scand.*, 1965, vol. 19, pp. 2369–72.
36. J. Kwon, L. Thuinet, M.N. Avettand-Fenoël, A. Legris, and R. Besson: *Intermetallics*, 2014, vol. 46, pp. 250–58.
37. J. Philibert: *Atom Movements, Diffusion and Mass Transport in Solids*, Les Éditions de Physique, Les Ulis, 1991.
38. A.D. Smigelkas and E.O. Kirkendall: *Trans. AIME*, 1947, vol. 171, pp. 130–42.